ENHANCING SENSITIVITY AND SELECTIVITY THROUGH AFFINITY RECEPTOR-DECORATED CHITOSAN-COATED GOLD NANOPARTICLES IN SURFACE PLASMON RESONANCE FOR SORTILIN BIOSENSING

SOPAN NANGARE and PRAVIN PATIL

Department of Pharmaceutical Chemistry, H. R. Patel Institute of Pharmaceutical Education and Research, Shirpur 425405, Dist: Dhule, Maharashtra, India
✉ *Corresponding author: P. O. Patil, rxpatilpravin@yahoo.co.in*

Received October 16, 2025

The present work reports a highly sensitive and selective surface plasmon resonance (SPR) biosensor for Sortilin (SORT), an important biomarker of coronary artery disease (CAD). In brief, chitosan (CH)-coated gold nanoparticles (Au-NPs) were fabricated through a layer-by-layer (LBL) nanoassembly on green-synthesized Au-NPs, followed by immobilization of anti-SORT antibodies using carbodiimide coupling. The CH coating provided abundant amine groups for efficient antibody attachment. Simultaneously, boron-doped graphene oxide (B-GO) nanosheets were deposited onto an amine-functionalized gold sensor chip to provide a large surface area and abundant active sites for anchoring the anti-SORT-decorated CH-coated Au-NP nanoassembly. The developed SPR biosensor exhibited a wide linear detection range from 400 to 0.1 ng/mL and a low detection limit of 6.09 pg/mL. Furthermore, the sensor demonstrated excellent stability, reproducibility, and real-time analytical capability, offering a label-free, eco-friendly, and minimally invasive platform for sensitive SORT detection.

Keywords: gold nanoparticles; sortilin, coronary artery disease; graphene oxide; boron doping; nanoassembly; surface plasmon resonance

INTRODUCTION

Coronary artery disease (CAD), also termed coronary atherosclerosis,[1] is a significant health issue related to cardiovascular disease, wherein the blood vessels narrow and harden, resulting in challenges in blood supply to the heart.[2] Artery blockage in CAD is primarily caused by abnormal lipids in the blood, which can lead to myocardial ischemia and myocardial necrosis.[3] The high prevalence of CAD contributes to elevated mortality and morbidity rates, while also imposing a substantial burden on the healthcare system.[2] Unfortunately, conventionally reported methods, such as coronary computed tomography (CT) imaging, coronary angiography,[1] immunoassays,[4] *etc*., suffer from various limitations, including high costs, hazards, and time-consuming procedures.[1] Additionally, CAD symptoms may not always manifest at an early stage.[2] Due to the severity of CAD, there is an urgent necessity to extend rapid and efficient CAD detection methods.[1] In this context, early-stage diagnosis based on the quantification of biomarkers in clinical samples can significantly reduce mortality.[4] The preference for state-of-the-art biosensors has garnered considerable attention for accurate, rapid, cost-effective, label-free, and simplified detection of disease-related biomarkers for early-stage diagnosis.[4,5]

Sortilin (SORT) is a relatively new biomarker that plays a crucial role in CAD. Essentially, it regulates lipid metabolism and is encoded by the SORT1 gene (a cardiovascular risk gene).[6] In the context of CAD, SORT significantly influences lipid metabolism in macrophages and the liver, contributing to CAD development.[3] Moreover, SORT may have a substantial impact on the *in vitro* diagnosis of other lipid-related health conditions.[6] Despite the pivotal role of SORT, limited attention has been given to the development of biosensors for its detection. Therefore, the use of advanced biosensors for SORT detection could offer a novel approach to early-stage diagnosis of CAD.

Presently, surface plasmon resonance (SPR) biosensor design has captured significant attention within the scientific community as a powerful tool for *in vitro* diagnosis of life-threatening health issues.[7] This heightened interest stems from a multitude of advantages associated with SPR biosensors, encompassing simplicity, rapid

detection, cost-effectiveness, high sensitivity, selectivity, robust stability, reproducibility, and ease of customization.[7,8] The phenomenon of SPR occurs in the presence of a sensorgram comprising a metal surface coated with a specific biomolecule serving as a recognition element, immersed in a medium (such as a vacuum or liquid). The identification of certain molecules that precisely match the receptor of this recognition element results in a change in the metal surface, leading to an angular shift. This shift occurs due to changes in the refractive index (RI) near the metal's surface. Both wavelength interrogation mode and angular interrogation mode are required to operate the SPR sensor. In this SPR phenomenon, the incident light's dispersion relation matches that of the surface plasmon at the resonance wavelength, resulting in a dip in reflectance. Notably, this reflectance dip is caused by the transfer of energy carried by photons incident on the surface plasmon and is highly sensitive to changes in the dielectric medium near the sensor surface.[9] In the case of traditional SPR-based biosensors, sensitivity and selectivity are major concerns. In brief, detecting analytes with low concentrations and low molecular masses can pose challenges for SPR-based biosensors.[10] To further enhance the performance of SPR biosensors, various types of nanomaterials have been explored.[7] Specifically, plasmonic nanomaterials like gold nanoparticles (Au-NPs) have been widely employed in SPR biosensors for immobilizing bioreceptors, leading to improved sensitivity and selectivity owing to their excellent optical properties.[5] Despite the significant advantages of bare metal nanoparticles, stability within the system remains a primary concern. Therefore, it necessitates suitable stabilizers to prevent aggregation.[11] Moreover, the immobilization of affinity bioreceptors on the surface of bare metal nanoparticles is a challenging task in SPR biosensors due to limited surface functionality.[10,11] Overall, these aforementioned challenges can be effectively addressed through the application of appropriate biopolymers coating the surface of Au-NPs.

The design of layer-by-layer (LBL) nanoassemblies using suitable types of cationic and anionic biopolymers has been reported for the development of biosensors.[12] Also, it is widely utilized in drug delivery applications.[13] The appeal of this approach lies in its simplicity, cost-effectiveness, and environmentally friendly processes. In this method, the coating of specific charge-containing polymer layers on the surface of metal nanoparticles results in the repulsion of nanoparticles, leading to the formation of stable particles.[14] In this case, a LBL nanoassembly offers several advantages, including improved surface area, conductivity, biocompatibility, optical/plasmonic properties, and uniform and abundant surface functionality. Overall, it contributes to enhanced biosensor performance. Furthermore, the LBL nanoassembly's preference is attributed to its softer surface area, which helps maintain biofunctionality and specific orientation.[12]

Chitosan (CH) is a polycationic biopolymer commonly employed in the design of LBL assemblies. Herein, CH provides a plethora of homogeneous amine functionalities that play a pivotal role in the immobilization of bioreceptors.[11] Additionally, CH offers mechanical stability and improved conductivity. To date, it has found applications in various types of biosensors for the detection of biomarkers related to different health issues, such as glucose, hydrogen peroxide, antigens, and others.[15] Therefore, the present study aims to utilize CH-coated Au-NPs in an LBL nanoassembly for the immobilization of affinity bioreceptors in an SPR biosensor, aiming to enhance the detection of SORT antigen.

The utilization of non-plasmonic two-dimensional carbon materials, such as graphene oxide (GO), has also been well-documented in SPR biosensors.[9] This is primarily due to their high surface area, abundant surface functionality, tuneability, excellent biocompatibility, and other favorable characteristics.[9,10] Furthermore, GO has the capability to induce shifts in SPR due to its optical properties and aids in the immobilization of biomolecules on the surface through various interactions, including both covalent and non-covalent bonding. Moreover, it contributes to the adjustment of the dielectric constant and band gap.[12] Furthermore, the modification of GO nanosheets using suitable heteroatoms offers the ability to customize the band gap and enhance the sensitivity of SPR biosensors.[16] To date, no LBL nanoassembly-decorated heteroatom (boron)-doped B-GO nanosheet-based SPR biosensor has been reported for the detection of SORT. Therefore, the objective of this study is to utilize B-GO nanosheets decorated on SPR biosensors to enhance the detection of the SORT antigen.

The present research work focused on designing a simplistic, highly sensitive, highly selective, label-free, cost-effective, environmentally friendly, stable, reproducible, and

speedy SPR biosensor for the recognition of the SORT antigen. To achieve this, an affinity bioreceptor (Anti-SORT) was immobilized on the surface of a CH and poly(sodium 4 styrene sulphonate) (PSS)-coated Au-NPs nanoassembly (Au-NPs@CH-PSS-CH@Anti-SORT nanobioconjugate). Here, CH provides an abundance of amine sites with a softer polymeric area suitable for the immobilization of affinity bioreceptors. It also imparts stability to the green-synthesized Au-NPs. This innovative design ensures uniform orientation of the anti-SORT bioreceptors, enhancing selectivity towards the SORT antigen. Additionally, B-GO was utilized as a non-plasmonic 2D carbon backbone for the immobilization of an Au-NPs@CH-PSS-CH@Anti-SORT nanobioconjugate (LBL nanoassembly). Here, B-GO's high surface area, high loading capacity, surface functional groups, and tunability contribute to boosting the performance of SPR for SORT detection. As a result, the combination of affinity Anti-SORT immobilized on CH-coated green-synthesized Au-NPs mediated nanoassembly, and their decoration on the B-GO nanosheets surface in the SPR biosensor offers lower detection limits and a wide linearity range for SORT. This advancement in SPR biosensor technology opens new possibilities for the detection of SORT and other biomarkers, facilitating *in vitro* and early-stage diagnosis of CAD and several other health-related diseases in the future.

EXPERIMENTAL

Materials

Sortilin (SORT) and Anti-SORT were procured from Sino Biological Inc., China. Graphite (>99%) nanosized flakes were generously provided as a gift sample by Asbury Carbons, located in New Jersey (NJ), USA. The highest purity sulfuric acid (H_2SO_4, 98%) and hydrogen peroxide (H_2O_2, 30% w/v) were obtained from Loba Chemie Pvt. Ltd., India (Mumbai). Chitosan (CH, MW: 160 kDa) was sourced from HiMedia Lab. Pvt. Ltd., India (Mumbai). Bovine serum albumin (BSA, purity >98%) was acquired from Sigma-Aldrich, USA. The reagent arsenal was further augmented with N-hydroxysuccinimide (NHS), 1-[3-(dimethylamino)propyl]-3-ethyl carbodiimide hydrochloride (EDC), gold (III) chloride hydrate (HAuCl4•H2O, 99.995%), and anionic poly(sodium 4 styrene sulphonate) [PSS, MW: ~70,000], all meticulously sourced from Sigma Aldrich, CO., St. Louis, USA. Avantor Performance Materials India Ltd. in Thane, India, provided the essential components, including 98% phosphoric acid (H_3PO_4), 35% hydrochloric acid (HCl), and HPLC-grade double-distilled water. Phosphate buffer saline (PBS) tablets with a pH of 7.4 were effortlessly sourced from Loba Chemie Pvt., Ltd. in Mumbai, India. The indispensable 99% isopropyl alcohol (IPA) came from Thermo Fisher Scientific India Pvt. Ltd. in Mumbai. Glycine hydrochloride (HPLC grade, ≥99%) was procured from Sigma Aldrich in Bangalore, India. The amine (NH_2) functionalized gold (Au)-coated sensor chip, a crucial component of a biosensor, was obtained from Nicoya Lifesciences in Canada. The ripe fruits of *Terminalia catappa* L. were meticulously collected from the local Shirpur vicinity. Additionally, the vital reagent potassium permanganate ($KMnO_4$, 99%, MW: 158.03) was supplied by Research Lab Fine Chem Industries in Mumbai, India.

Methods

Synthesis of boron-doped GO (B-GO) nanosheets

The synthesis of B-GO nanosheets was carried out using a previously reported method.[17] In brief, the synthesis of GO nanosheets began with the preparation of GO from graphite flakes powder, following a modified Hummers method. Initially, a mixture of H_2SO_4 and H_3PO_4 (108 mL: 12 mL) was prepared in a clean glass beaker. The resultant acid mixture was uniformly mixed at 250 rpm for 15 min using a stirrer. Once both acids were completely mixed, 900 mg of nanosized graphite flakes were gradually added to the acidic mixture while stirring continuously at 200 rpm for 20 min at 20 °C. Once a consistent blending of graphite flakes with the acids was achieved, 4.64 g of $KMnO_4$ was gradually added with continuous stirring at 450 rpm. The final blend was left to react for 6 h until it turned into a dark green color. After the 6-h reaction period, 2.70 mL of H_2O_2 was gradually added to the dark green graphite mixture to remove any remaining $KMnO_4$. During this step, the mixture was stirred at 500 rpm for the following 10 min at 25 °C to reduce the process temperature. Subsequently, the resulting green-yellow dispersion of GO was gathered and subjected to a centrifugation process at 10,000 rpm and 20 °C for 50 min, employing a mixture of HCl and DDW in a 2:6 ratio for washing. This washing process was repeated three times. The obtained GO dispersion was then subjected to probe sonication (3 cycles of 5 seconds each) to obtain nanosized GO sheets. Finally, the remaining GO was dried using a vacuum oven at 50 °C to ensure complete drying of the GO nanosheets.

B-GO was prepared using the previously reported procedure.[18] In this process, 2 g of GO nanosheets were dispersed in 100 mL of DDW. Subsequently, boric acid was added to the GO nanosheet dispersion at a 1:0.1 ratio, followed by ultrasonication. The mixture was then stirred for 8 h at 500 rpm at 80 °C. Afterward, the resulting mixture was heated in a Teflon tube autoclave for 12 h at 180 °C. Upon completion of the reaction, the B-GO nanosheets were washed with DI water to remove any unreacted boric acid. Finally, the B-GO nanosheets

were dried using a freeze-drying process, as described in previously reported literature.[19]

Green synthesis of Au-NPs

The green synthesis of Au-NPs was achieved using an environmentally friendly approach.[20] To briefly describe the process, 50 g of ripe fruits from *Terminalia catappa* L. were collected as waste from the Shirpur local market. The fruits were cleaned with deionized water, and their epicarp (outer skin) was separated and cut into small pieces. The epicarp pieces were then dried in a laboratory programmable hot air oven at 50 °C and subsequently ground into a powder. For the extraction of biomolecules required for the synthesis of Au-NPs, 10 g of epicarp powder was mixed with 200 mL of deionized water (DDW) and subjected to extraction at 50 °C for 1 h. The mixture was then filtered using filter paper to separate the undissolved residue from the extracted solution. The resulting extract was concentrated through cold centrifugation at 12,000 rpm for 30 min and further filtered using a 0.22 µm-sized membrane filter. Finally, the filtrate was stored at a low temperature for subsequent use in the synthesis of Au-NPs. The one-pot synthesis of Au-NPs was achieved using the obtained extract from the ripe fruits of *Terminalia catappa* L. Specifically, 5 mL of the extract was mixed with 200 mL of $HAuCl_4$ solution (7 mM) in a volumetric flask. This mixture was continuously stirred at 1000 rpm at 50 °C using a laboratory magnetic stirrer. The progress of Au-NP formation was monitored throughout the 24 h synthesis period. After completion of 24 h, the resulting dispersion of Au-NPs was subjected to freeze-drying using a previously established method.[19] The resulting freeze-dried Au-NPs powder was then utilized for subsequent spectral characterizations and the design of LBL nanoassemblies.

Design of Anti-SORT immobilized CH-based Au-NPs nanoassembly

In this step, the LBL-based nanoassembly was prepared using a previously reported method.[10,11,14] To summarize, 300 mg of freeze-dried Au-NPs were dispersed in 50 mL of deionized water (DI water). Simultaneously, 1% CH and 1% PSS solutions were prepared as cationic and anionic coating agents, respectively. For the 1% CH solution, 1 g of CH was dissolved in 100 mL of a dilute 1% (v/v) acetic acid solution, whereas the 1% PSS solution was prepared using DDW. These ready solutions were subjected to cold centrifugation at 15,000 rpm to remove any undissolved matter and then membrane-filtered to obtain pure coating agent solutions. To create the first layer of the assembly, 45 mL of the Au-NPs dispersion was mixed with 10 mL of the 1% CH solution. The Au-NPs-CH nanoassembly was stirred continuously at 100 rpm at room temperature to facilitate electrostatic interactions between the negatively charged Au-NPs and the cationic CS. Subsequently, the resulting Au-NPs-CH nanoassembly was centrifuged at 15,000 rpm for 45 min at 25 °C to separate unreacted CH from the nanoassembly. The charge of the obtained nanoassembly was confirmed, and it was then subjected to lyophilization. For the deposition of the second layer consisting of the negatively charged coating agent, 200 mg of Au-NPs-CH nanoassembly was dispersed in 50 mL of DI water. Subsequently, 10 mL of 1% PSS solution was added to the 45 mL of Au-NPs@CH nanoassembly dispersion. The resulting mixture, known as Au-NPs@CH-PSS, was stirred at 100 rpm for 3 h at 22 °C to promote electrostatic interactions between the positively charged Au-NPs-CH nanoassembly and the negatively charged PSS. Following this, the Au-NPs@CH-PSS nanoassembly was centrifuged to remove any unreacted PSS. Finally, the dispersion of the Au-NPs@CH-PSS nanoassembly was freeze-dried using a previously documented method. For the deposition of the third layer of CH onto the surface of the Au-NPs@CH-PSS nanoassembly, 100 mg of the Au-NPs@CH-PSS nanoassembly was dispersed in 50 mL of DI water. The 45 mL of Au-NPs@CH-PSS nanoassembly was mixed with 10 mL of 1% CH solution. The same process as discussed for the first layer deposition was followed to obtain the Au-NPs@CH-PSS-CH nanoassembly.

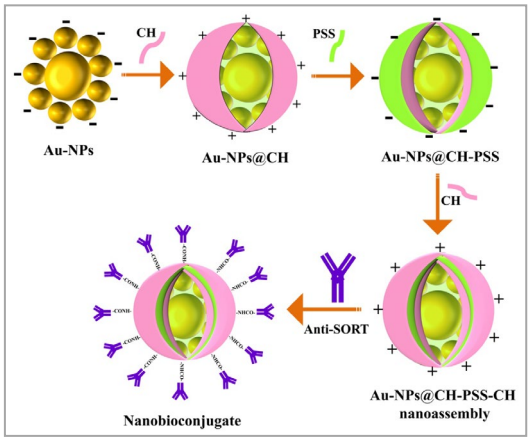

Scheme 1: Design of Anti-SORT immobilized CH-based Au-NPs nanoassembly

Ultimately, the Au-NPs@CH-PSS-CH nanoassembly was lyophilized using a laboratory freeze dryer. Scheme 1 represents the design of Anti-SORT immobilized CH-based Au-NPs nanoassembly. The final Au-NPs@CH-PSS-CH nanoassembly was further employed for the immobilization of bioreceptors to create the final SPR biosensor for the detection of SORT.

Spectral characterization

The ultraviolet (UV) visible (Vis) analysis was performed using a UV spectrophotometer (UV-1800, Shimadzu, Japan) with a programmed wavelength range of 200 nm to 800 nm and a quartz cuvette (path length cm). The surface properties of the acquired nanomaterials were verified through Attenuated Total Reflectance-Fourier Transform Infrared spectrophotometry (ATR FTIR) using the Bruker Alpha II instrument with a Platinum ATR attachment. Particle size and zeta potential analysis were conducted using a particle size analyzer (Nanoplus 3, Micromeritics, USA). The percentage composition of the formulated nanomaterials was verified through energy-dispersive X-ray analysis (EDAX) using the Oxford XMX N instrument, which offers a resolution of 136 eV and a 30 mm^2 detector area. Additionally, surface morphology analysis of the nanomaterials was performed using scanning electron microscopy (SEM) with a JEOL JSM-6390LV instrument from Tokyo, Japan, featuring an accelerating voltage range between 0.5 kV and 30 kV. Changes in defects in the graphitic structure (the 'D' band and the 'G' band) were determined using a Raman spectrometer (Confocal micro-Raman spectrometer, Horiba, HR800-UV). The particle size and shape of the obtained nanomaterials were determined using high-resolution transmission electron microscopy (HR-TEM, Jeol/JEM 2100) with LaB_6 as an electron source at 200 kV. The characteristics of the acquired nanomaterials were established through powdered X-ray diffraction (PXRD) using the Bruker D_8 Advance instrument. Furthermore, the surface functionality was authenticated via X-ray photoelectron spectroscopy (XPS) using the Physical Electronics PHI 5000 Versa Probe III.

Synthesis of Au-NPs@CH-PSS-CH@Anti-SORT nanobioconjugate

In this step, Anti-SORT was immobilized on the surface of the Au-NPs@CH-PSS-CH nanoassembly using carbodiimide chemistry. Here, 5 mg of Au-NPs@CH-PSS-CH nanoassembly was suspended in 10 mL of nuclease-free water (filtered through a 0.45 µm filter). Subsequently, the carboxylic functionality of Anti-SORT was activated using 100 mM EDC and 25 mM NHS (1:1) at 10 °C. Then, 200 µL of the antibody was mixed with 5 mL of the dispersion of Au-NPs@CH-PSS-CH nanoassembly (500 µg/mL) for immobilization, wherein the activated carboxylic functionality reacts with the amine functionality of CH-containing Au-NPs@CH-PSS-CH nanoassembly, forming the Au-NPs@CH-PSS-CH@Anti-SORT nanobioconjugate.

Detection of SORT using a designed SPR biosensor

In this step, the detection of SORT was performed using a designed LBL nanoassembly and a heteroatom-doped GO-based SPR affinity biosensor. In short, an amine-functionalized gold-coated sensor chip was placed in OpenSPR. The surfaces of both the sensor chip and the sample loop were cleansed by flushing them with 150 µL of phosphate buffer at pH 7.4, followed by nuclease-free water and IPA at a flow rate of 100 µL/min. After washing, 50 µg/mL of B-GO nanosheet dispersion was prepared in nucleae-free water. These B-GO nanosheets were activated with EDC (0.4 M) followed by NHS (0.1 M) to activate the carboxylic functionality on their surface. These activated B-GO nanosheets (50 µg/mL) were then injected (flow rate: 100 µL/min) into the sample port to immobilize them on the surface of the procured amine-functionalized gold-coated SPR chip, forming an amide bond. After confirmation, the activated Au-NPs@CH-PSS-CH@Anti-SORT nanobioconjugate (200 ng/mL) was injected at a regulated flow rate of 100 µL/min to immobilize it on the activated carboxylic functional groups present on the B-GO nanosheets. This immobilization was achieved via carbodiimide chemistry using EDC/NHS 1:1) at a programmed temperature below 25 °C. Following immobilization of the nanobioconjugate, washing was performed using pH 7.4 PBS to remove any non-bound Au-NPs@CH-PSS-CH@Anti-SORT nanobioconjugate. The free-activated carboxylic functionality was then masked using BSA as a blocking agent. During this step, 200 µg/mL of BSA was introduced into the system through the sample port twice, maintaining a flow rate of 100 µL/min. Subsequently, washing was performed (flow rate: 50 µL/min) using PBS at pH 7.4 to remove unbound BSA from the surface of the SPR sensor chip.

Simultaneously, different concentrations of the SORT antigen were prepared within the range of 500 ng/mL, 400 ng/mL, 300 ng/mL, 200 ng/mL, 100 ng/mL, 50 ng/mL, 10 ng/mL, 1 ng/mL, 0.8 ng/mL, 0.6 ng/mL, 0.4 ng/mL, 0.2 ng/mL, 0.1 ng/mL, and 0.01 ng/mL in pH 7.4 PBS in sterilized tubes. Then, 400 ng/mL of SORT (200 µL) was injected via the sample port (flow rate: 100 µL/min). Here, the total association time for the antigen and antibody was monitored. After the completion of the association process, it was observed for 60 seconds, followed by a regeneration process in which the unbound antigen was removed using 200 µL of 10 mM glycine hydrochloride (pH 1.2) as a washing agent (dissociation time: 100 seconds). A similar process was employed for different concentrations of the SORT antigen under controlled parameters. Scheme 2 represents the Au-NPs@CH-PSS-CH@Anti-SORT nanobioconjugate (nanoassembly) immobilized on B-GO nanosheets decorated SPR biosensor for the detection of SORT antigen. Finally, linearity was

calculated using a SPR response based on the designed SPR biosensor versus the concentration of the SORT antigen. Following that, the limit of detection (LOD) and limit of quantification (LOQ) were determined using the following formulas:

$$LOD = 3.3 \times \frac{SD}{S} \quad (1)$$

$$LOQ = 10 \times \frac{SD}{S} \quad (2)$$

where 'SD' indicates the standard deviation, whereas 's' represents the slope obtained from the calibration curve for LOD.

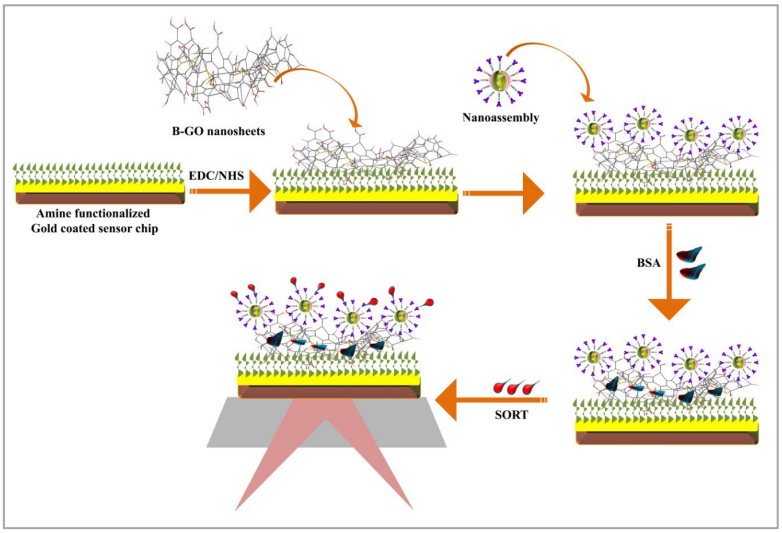

Scheme 2: Au-NPs@CH-PSS-CH@Anti-SORT nanobioconjugate (nanoassembly) immobilized on B-GO nanosheets decorated SPR biosensor for detection of SORT antigen

Selectivity analysis of the SPR biosensor

The selectivity analysis of the designed SPR biosensor for SORT was conducted by testing its response to a diverse range of interfering substances. In summary, various interfering agents, such as bovine serum albumin, cholesterol, lysine, lactoferrin, protease, calcium, bicarbonate, sodium, potassium, urea, glycine, and aspartic acid were selected to mimic the composition of a representative blood sample. A concentration of 100 ng/mL for each interfering agent was prepared in separate clean tubes. Simultaneously, SORT antigen (100 ng/mL) was prepared to validate the selectivity of the biosensor against these selected interfering agents. A volume of 150 µL of the prepared sample was injected via the sample port, and the response was assessed using the programmed parameters outlined above. The same process was repeated for each interfering agent individually. Additionally, a mixture of all interfering agents was analyzed for its potential interference. Finally, the SORT antigen was injected via the sample port to compare its response against the other interfering agents.

Stability and reproducibility of the designed SPR biosensor

After confirming sensitivity and selectivity, the designed SPR biosensor underwent stability, reproducibility, and spiked sample analysis testing. In brief, a stability assessment of the designed SPR biosensor was conducted for detecting the SORT antigen. Specifically, a concentration of 200 fg/mL SORT antigen was injected via the sample port at various time intervals, including 1 h, 2 h, 4 h, 6 h, 8 h, 12 h, 20 h, and 24 h (n = 3). The response of the designed SPR biosensor to the SORT antigen was monitored at these specified time intervals to ensure its stability. The reproducibility of the designed SPR biosensor was achieved using multiple SPR biosensors (n = 5). In this case, 200 fg/mL SORT antigen was introduced via the sample port with the parameters mentioned above. The percentage of relative standard deviation (% RSD) was computed and reported to validate the stability and reproducibility of the expected SPR biosensor.

Spiked sample analysis of the designed SPR biosensor

To ensure the practical applicability of the designed SPR biosensor, spiked sample analysis was conducted. In this analysis, various concentrations (0.4 ng/mL, 0.6 ng/mL, and 0.8 ng/mL) of SORT antigen were prepared. Simultaneously, plasma samples were obtained from healthy albino Wistar rats (Proposal approval no. MPC/IAEC/14/2021). The response for the collected samples was confirmed to verify the presence of the SORT antigen in non-spiked samples. Once confirmed, the prepared SORT antigen concentrations were spiked into 1 mL of plasma samples separately using Eppendorf tubes. Subsequently, these spiked samples were sequentially injected to obtain the response for SORT antigen, employing the prepared SPR biosensor with programmed process parameters, as detailed

above. The % recovery and % RSD of the SORT antigen were calculated to validate the practical applicability of the designed SPR biosensor in clinical samples.

RESULTS AND DISCUSSION

Spectral characterization of B-GO nanosheets

To confirm the synthesis of B-GO, the HR-TEM, zeta potential, XPS, and Raman analysis were performed. In brief, the surface morphology of the prepared B-GO nanosheets was confirmed using HR-TEM analysis. Herein, the HR-TEM analysis revealed the formation of two-dimensional, nanosized, and flexible thin sheets in the B-GO nanosheets. Additionally, the surface of these nanosheets exhibited a wrinkled and undulated structure due to the exfoliation process followed by boron doping (Fig. 1A). Figure 1B shows the zeta potential of B-GO nanosheets. Shortly, zeta potential analysis of B-GO nanosheets yielded a value of -27.56 mV. This result confirms the presence of oxygen-based functionalities, such as carboxylic, epoxy, and hydroxyl groups, on the surface of B-GO nanosheets. Additionally, it demonstrates good electrostatic stability in aqueous dispersion systems. Figure 1C shows the Raman spectra of B-GO nanosheets. In short, the Raman analysis of B-GO nanosheets revealed a 'D' band peak at 1409.98 cm^{-1} and a prominent 'G' band peak at 1676 cm^{-1}. The relative intensity of I_D to I_G (I_D/I_G) was found to be less than 1, confirming the presence of oxygen-based functional groups within the graphite layers.[16] These functional groups contribute to the hydrophilic nature of B-GO nanosheets.

The functionality of B-GO nanosheets was assessed using XPS analysis (Fig. 2). To summarize, the XPS survey scan spectra exhibited dominant peaks at 190 eV, 282.5 eV, and 529.5 eV, confirming the presence of B1s, C1s, and O1s in the synthesized B-GO nanosheets (Fig. 2A). After this confirmation, the deconvolution of XPS spectra was performed. Herein, the high-energy deconvoluted spectrum of B1s displayed dominant peaks at 187.74 eV, 189.47 eV, and 190.49 eV, providing evidence for the boron doping of SP^2 and SP^3 carbon atoms (Fig. 2B). Similarly, the high-energy deconvoluted spectrum of C1s exhibited dominant peaks at 281.34 eV, 282.44 eV, 283.57 eV, and 286.04 eV, confirming the presence of carboxylic functionality in the B-GO nanosheets (Fig. 2C). Finally, the high-energy deconvoluted XPS peaks of O1s at 528.32 eV, 529.47 eV, and 531.24 eV confirmed the presence of oxygen-based functionality in the B-GO nanosheets (Fig. 2D). Overall, the XPS analysis verified the elemental composition of the B-GO nanosheets.[21]

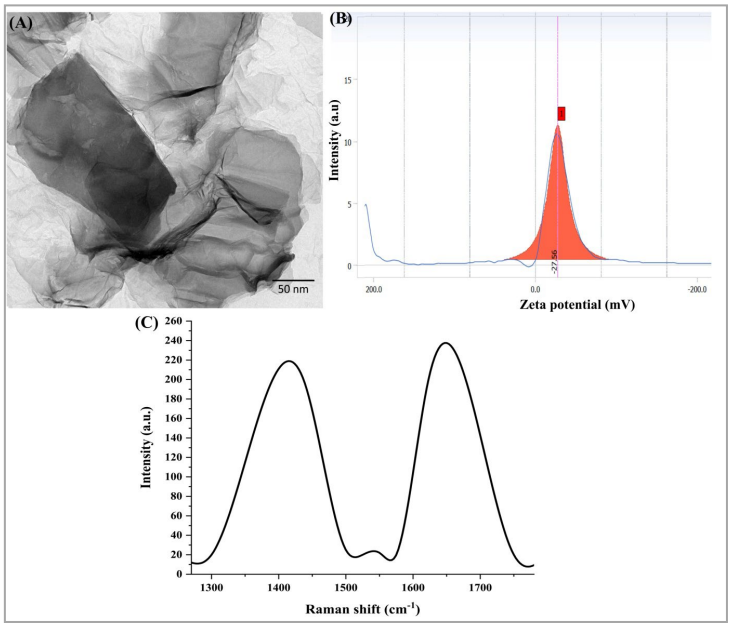

Figure 1: (A) HR-TEM image of B-GO nanosheet; (B) Zeta potential of B-GO nanosheets; (C) Raman spectra of B-GO nanosheets

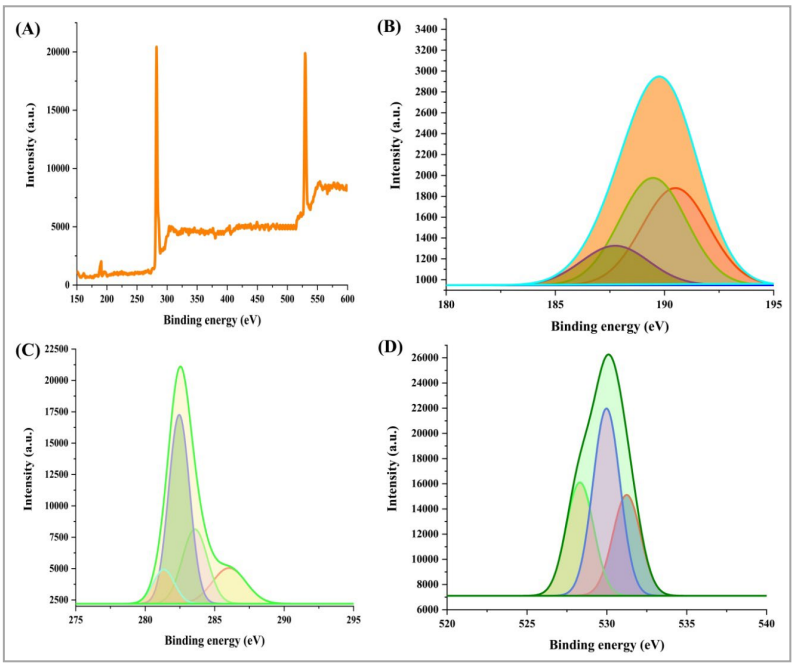

Figure 2: (A) Presentation of XPS survey scan spectra of B-GO nanosheets; (B) Deconvoluted XPS high-resolution peak of Bls; (C) C1s; and (D) O1s

Spectral characterization of green-synthesized Au-NPs

In this step, the green-made Au-NPs were examined using several spectral characterizations. In brief, the visual observation involves the green synthesis of purple-colored Au-NPs.[22] This transformation occurs when the yellow-colored chloroauric acid is mixed with an extract from the ripe fruit epicarp of *Terminalia catappa* (Fig. 3A). Simultaneously, the obtained Au-NPs were confirmed using UV-Vis analysis. In this UV Vis analysis, the emergence of a new peak at 532.5 nm confirmed the synthesis of Au-NPs (Fig. 3B).[23] Notably, the peaks corresponding to the extract and chloroauric acid were suppressed due to the interaction between gold ions and the biomolecules present in the extract. Following the confirmation via UV-Vis analysis, we determined the particle size, polydispersity index (PDI), and zeta potential. In short, the particle size and PDI of the Au-NPs synthesized through the green method were both found to be 52.2 nm and 0.26, respectively.[24] Thereby, it affirms the synthesis of uniformly dispersed and nanosized Au-NPs (Fig. 3C). Additionally, the zeta potential of the obtained Au-NPs was measured at - 20.70 mV, confirming their excellent stability in aqueous systems (Fig. 3D).[25] In this, the negative zeta potential of the nanoparticles can be attributed to the presence of carboxylic biomolecules in the extract, which play a pivotal role in reducing, capping, and stabilizing the Au-NPs. Overall, it ensured the synthesis of Au-NPs using the green method.

After initial confirmation, the surface morphology of Au-NPs was confirmed using SEM analysis. Here, Figure 4A depicts the SEM image of green-synthesized Au-NPs, revealing the formation of spherical-shaped nanoparticles with nanometer-scale particle sizes and rough surfaces.[26] Here, the rough surface was found to be because of the deposition of biomolecules as a stabilizing agent on the surface of Au-NPs. In addition, further verification of the actual diameter of Au-NPs was conducted using HR-TEM analysis.[25] The elemental composition of Au-NPs was confirmed via EDX analysis, resulting in weight percentages of 19.40 wt%, 40.15 wt%, 32.30 wt%, and 8.15 wt% for gold, carbon, oxygen, and nitrogen, respectively (Fig. 4B). This confirmed the presence of biomolecules in the extract responsible for Au-NP synthesis. The surface functionality of the obtained Au-NPs was examined using FT-IR analysis. As an output, the FT-IR analysis of the freeze-dried Au-NPs displayed peak vibrations at various wavenumbers such as 3351.12 cm^{-1}, 1656.08 cm^{-1}, 1371.19 cm^{-1}, and 1035.05 cm^{-1}, confirming the occurrence of OH/NH stretching vibrations, C=O vibrations, NH bending vibrations, and C-O stretching vibrations, respectively (Fig. 4C). In conclusion, FT-IR

analysis established the presence of carboxylic functionality within the extract, which plays a crucial role in the synthesis of Au-NPs.[25,27] In a nutshell, it assured the synthesis of green-made, nanosized, pure forms of Au-NPs.

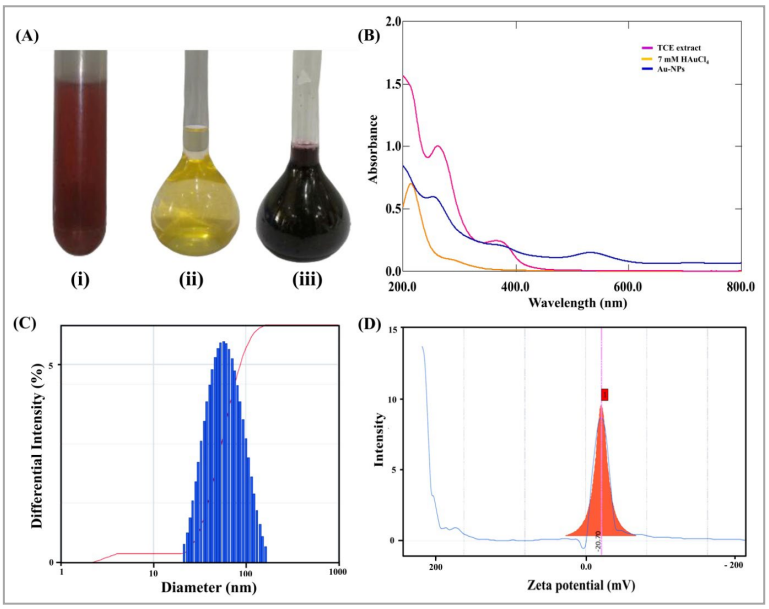

Figure 3: (A) Images of extract (i), chloroauric acid (ii), and green-prepared Au-NPs; (B) UV-Vis graph of extract (i), chloroauric acid (ii), and green-prepared Au-NPs; (C) Particle size assessment of green-made Au-NPs; (D) Zeta potential analysis of green-made Au-NPs

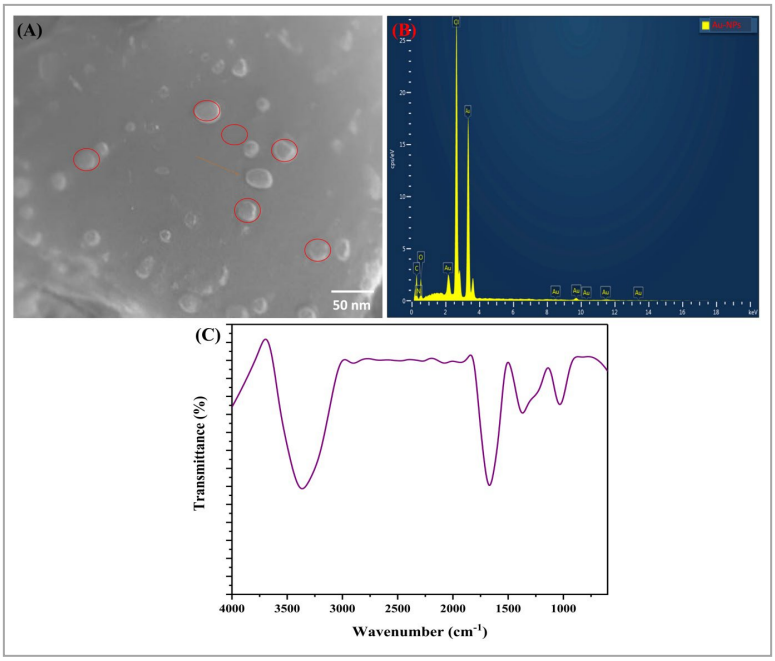

Figure 4: (A) SEM image of green-synthesized Au-NPs; (B) EDX spectrum of green-synthesized Au-NPs; (C) FT-IR spectrum of green-synthesized Au-NPs

The solid form of the green-made Au-NPs was confirmed using PXRD analysis. In brief, Figure 5A illustrates the diffractogram of green-synthesized Au-NPs. In summary, the intensity peak ranging from 2θ = 28.46°, 38.36°, 40.65°, 44.56°, 50.27°, 58.76°, 64.71°, 66.47°, 73.73° and 77.42° signifies the formation of crystalline Au-NPs. To verify the actual diameter, HR-TEM

analysis was carried out, as shown in Figure 5B and C. In brief, the particle size range of Au-NPs spans from 14.54 nm to 32.36 nm, with an average particle size of 24.06 nm (N = 20, Software: ImageJ). Furthermore, these Au-NPs exhibited a consistent spherical shape.[24] In conclusion, HR-TEM analysis confirmed the formation of non-aggregated nanosized Au-NPs.

Figure 6A illustrates the XPS spectrum of green-synthesized Au-NPs. In summary, the survey scan spectrum of these Au-NPs reveals binding energies of 86.5 eV, 284 eV, 399 eV, and 531 eV for gold, carbon, nitrogen, and oxygen, respectively. Therefore, it ensures that the green synthesis of Au-NPs results in a composition consisting exclusively of gold (Au), nitrogen (N), carbon (C), and oxygen (O), with the absence of any other potentially toxic components for biomolecules, such as antigens and antibodies. This plays a crucial role in preserving the biofunctionality of these biomolecules and consequently enhances the overall performance of the biosensor. Next, Figure 6B presents the high-resolution deconvoluted spectrum of gold, where the observed binding energy at 84.37 eV and 88.66 eV confirms the presence of Au 4f(7/2) and Au 4f(5/2), respectively. Additionally, Figure 6C shows the high-resolution deconvoluted spectrum of Cls, with binding energy at 284.41 eV, 285.46 eV, and 286.70 eV confirming the presence of C-C, C-N and C=O, respectively. Figure 6D displays the high-resolution deconvoluted spectrum of O1s, and binding energy at 531.21 eV and 532.36 eV confirms the presence of C=O and C-O, respectively. Finally, Figure 6E demonstrates the high-resolution deconvoluted spectrum of N1s, where the binding energy at 399 confirms the presence of C-N.[10,28] In conclusion, the XPS analysis confirms the presence of carboxylic functionality on the surface of green-made Au-NPs.

Spectral characterization of LBL based nanoassembly

In this step, the CH and PSS layers on Au-NPPs were optimized by taking into account parameters such as the plasmon shift and practical feasibility. The choice of CH layers on Au-NPs (Au-NPs@CH-PSS-CH) was guided by both observed plasmon shifts and established laboratory protocols. Remarkably, we observed a redshift in the Au-NPs containing plasmon band for the initial three layers deposited (AuNPs@CH-PSS-CH), indicating successful 'CH' and 'PSS' adsorption onto the colloidal surface.

This shift is attributed to subtle alterations in the local RI, reflected in changes in the extinction and scattering spectra.

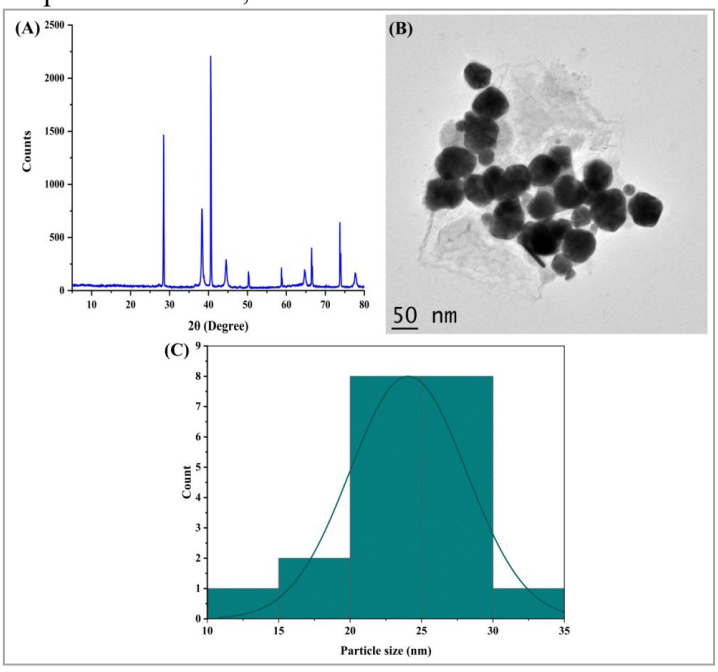

Figure 5: (A) Diffractogram of Au-NPs; (B) HR-TEM image of prepared Au-NPs; (C) Particle size distribution of green-synthesized Au-NPs (Software: ImageJ)

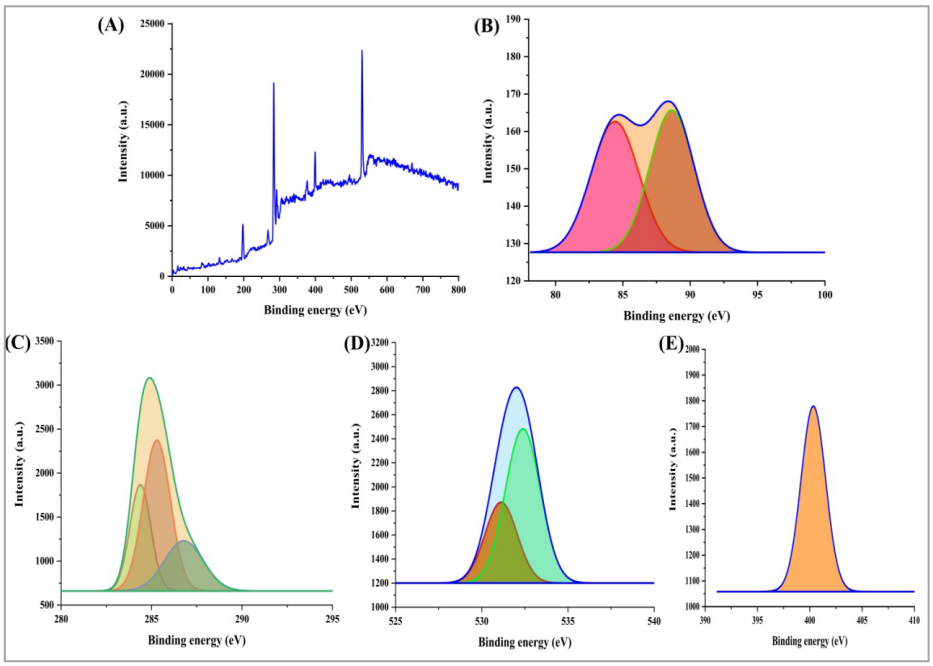

Figure 6: (A) Survey scan XPS spectra of prepared Au-NPs; (B) Deconvoluted high-resolution peak of Au; (C) C1s; (D) O1s; and (E) N1s

Notably, the redshift of the green synthesized Au-NPs plasmon band persists up to three layers, suggesting a transient modification in the local RI. However, beyond three layers, the plasmon band wavelength stabilizes, indicative of a permanent change in the local RI. Consequently, we selected the AuINPs@CH-PSS-CH configuration for the development of our bioconjugate.[14] Furthermore, we noted that the preparation and purification process of AuNPs@CH-PSS-CH-PSS-CH is more time-intensive compared to AuNPs@CH-PSS-CH, underscoring the practical considerations in our choice.

Then, the synthesis of Au-NPs@CH, Au-NPs@CH-PSS, and Au-NPs@CH-PSS-CH nanoassemblies was confirmed through zeta potential analysis and particle size measurements. At first, Figure 7A presents the zeta potential values of Au-NPs, CH, PSS, Au-NPs@CH, Au-NPs@CH-PSS, and Au-NPs@CH-PSS-CH nanoassemblies. Specifically, the zeta potential of Au-NPs, CH, and PSS was determined to be – 20.52 ± 2.1 mV, + 37.58 ± 1.98 mV, and – 39 ± 1.1 mV, respectively. In this context, the detrimental impact of green-synthesized Au-NPs can be attributed to the deposition of carboxylic functionality from the extract, which serves as both a reducing and stabilizing agent. Furthermore, the positive zeta potential of CH arises from the amine functionality present on its surface, while the negative zeta potential of PSS is primarily influenced by the presence of SO_3^-. At first, after the deposition of cationic CH onto the surface of negatively charged Au-NPs, the zeta potential was found to be + 27.89 ± 2.2 mV, confirming the formation of stable Au-NPs@CH in an aqueous system.[10] In the subsequent step involving the Au-NPs@CH-PSS nanoassembly, a change in zeta potential was observed following the deposition of negatively charged PSS onto the surface of positively charged Au-NPs@CH. Consequently, the zeta potential of Au-NPs@CH-PSS was measured to be -31.22 ± 2.2 mV,[29] affirming the successful creation of a stable assembly in an aqueous environment. Finally, with the deposition of CH onto the negatively charged Au-NPs@CH-PSS, the zeta potential shifted to the positive side. In this case, the zeta potential of the Au-NPs@CH-PSS-CH nanoassembly was determined to be + 24.45 ± 1.19 mV. In summary, zeta potential analysis of these nanoassemblies confirmed the formation of a stable, LBL-based Au-NPs@CH-PSS-CH nanoassembly.

After confirming the zeta potential of the LBL assemblies, particle size analysis was conducted. Here, Figure 7B illustrates the particle size analysis of Au-NPs, Au-NPs@CH, Au-NPs@CH-PSS, and Au-NPs@CH-PSS-CH nanoassemblies. The particle size for Au-NPs, Au-NPs@CH, Au-NPs@CH-PSS, and Au-NPs@CH-PSS-CH nanoassemblies was measured at 65.22 ± 2.29 nm,

79.21 ± 3.99 nm, and 81.42 ± 1.45, respectively (Fig. 7B). Additionally, the polydispersity index for Au-NPs, Au-NPs@CH, Au-NPs@CH-PSS, and Au-NPs@CH-PSS-CH nanoassemblies was determined to be 0.32, 0.29 nm, and 0.26, respectively. Notably, the deposition of cationic and anionic polymeric layers on the exterior of green-synthesized Au-NPs resulted in an increase in particle size in the LBL nanoassemblies. Overall, the particle size analysis confirmed the successful deposition of 'CH' and 'PSS' onto the surface of Au-NPs.

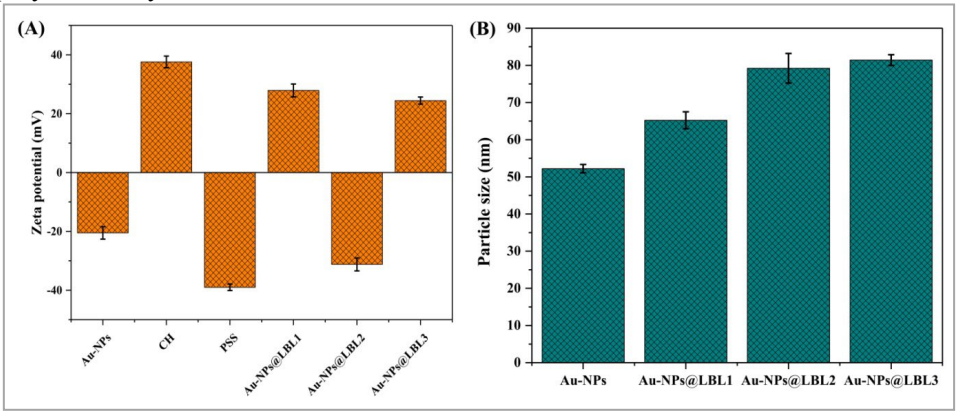

Figure 7: (A) Zeta potential and (B) Particle size analysis of Au-NPs@CH (Au-NPs@LBL1), Au-NPs@CH-PSS (Au-NPs@LBL2), and Au-NPs@CH-PSS-CH (Au-NPs@LBL3) nanoassemblies

Detection of SORT using designed SPR biosensor

The sensitivity enhancement of SPR biosensors has been achieved through various approaches, notably leveraging advanced nanomaterials such as metal nanoparticles, carbon-based nanomaterials, and metal oxides. In essence, these nanomaterials play a pivotal role in improving biosensor performance by their optical and electrical properties. Additionally, their biocompatibility, surface tunability, and other merits contribute significantly to enhancing SPR sensitivity.[5] The utilization of affinity receptors, such as antibodies, has also been reported in the design of SPR biosensors. Here, the use of affinity bioreceptors plays a crucial role in targeting specific analytes within complex samples owing to their high affinity towards the target analyte.[7] Recently, the design of LBL assemblies for the immobilization of antibodies has been documented to enhance both sensitivity and selectivity in SPR biosensors. In this method, the design of LBL nanoassemblies utilizing suitable types of cationic and anionic biopolymers is based on principles of simplicity, cost-effectiveness, and environmentally friendly processes.[14] The process involves coating specific charge-containing polymer layers onto the surface of metal nanoparticles, resulting in the repulsion of nanoparticles and the formation of stable metal nanoparticle assemblies.[14] The use of LBL nanoassembly in constructing SPR biosensors offers several advantages, including improved surface area, conductivity, biocompatibility, and optical/plasmonic properties, as well as uniform and abundant surface functionality, all of which contribute to enhanced biosensor performance. Furthermore, the preference for LBL nanoassembly is attributed to its softer surface area, which aids in maintaining biofunctionality and specific orientation.[12]

Based on these strategies, we detected the SORT antigen using a custom-designed SPR biosensor. To summarize, we immobilized carboxylic functional group-activated B-GO nanosheets onto the exterior of an amine-modified gold-coated glass chip through carbodiimide chemistry. This immobilization process involved creating amide bonds between the amine groups on the glass chip and the triggered carboxylic functionalities of the nanosheets, effectively anchoring them onto the sensor surface. Subsequently, we immobilized the Au-NPs@CH-PSS-CH@Anti-SORT nanobioconjugate onto the surface of the B-GO nanosheets. To complete this process, we blocked any remaining activated carboxylic functional groups using BSA as a masking agent. Following the final setup, we introduced SORT antigen concentrations ranging from lower to higher concentrations, resulting in a concentration-dependent change in the SPR sensorgram. As a result, our designed SPR

biosensor demonstrated an extensive linear range, spanning from 400 ng/mL to 0.1 ng/mL (Fig. 8A and B). The calibration curve (Fig. 8C) provides the y = 0.184x - 4.167 (R^2 = 0.99).

Furthermore, we determined the LOD and LOQ to be 6.09 pg/mL and 18.47 pg/mL, respectively. It is noteworthy that our preference for the designed SPR biosensors led to enhanced sensitivity due to the utilization of advanced strategies.[7] In essence, this enhancement can be attributed to the synergistic combination of the Au-NPs@CH-PSS-CH-based nanoassembly, environmentally-friendly Au-NPs, and B-GO nanosheets. Our design primarily involved the development of a polymeric LBL-based nanoassembly, consisting of CH and PSS on the surface of green-synthesized Au-NPs. Herein, the incorporation of CH provided numerous amine sites crucial for the immobilization of Anti-SORT. This Au-NPs@CH-PSS-CH-based nanoassembly approach significantly facilitated the maximal immobilization of the Anti-SORT antibody onto the green-synthesized Au-NP surface. Moreover, direct immobilization onto the Au-NP surface might lead to adsorption of Anti-SORT through weak interactions, potentially resulting in detachment during subsequent washing steps, thereby affecting the sensitivity of the SPR biosensor for SORT antigen.[14] To circumvent this issue, we employed the LBL assembly method, wherein CH offered homogeneous functional groups for the covalent immobilization of antibodies. This was achieved through the formation of bonds between the amino groups of CH and the carboxylic functionalities of antibodies using EDC/NHS chemistry.[12]

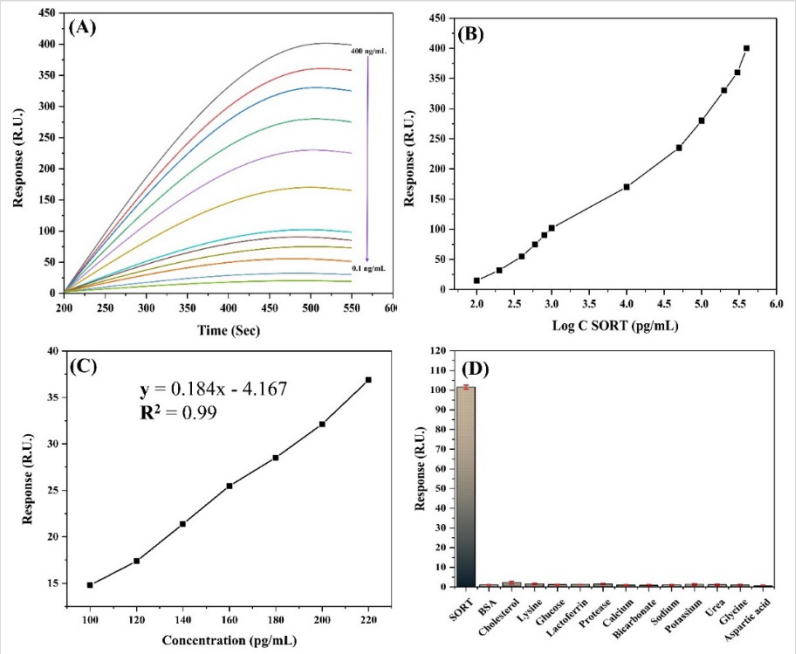

Figure 8: (A) SPR sensogram of SORT antigen using a designed SPR biosensor; (B) Linearity graph for concentration of SORT antigen *vs.* SPR response; (C) Calibration curve of SORT antigen vs response; (D) Selectivity analysis of SPR biosensor for detection of SORT antigen in the presence of different interfering agents

Furthermore, the role of the LBL assembly extends to providing a biocompatible polymer soft layer, which contributes to maintaining bioreceptor orientation and biofunctionality better than bare metal nanoparticles alone. Thus, the CH-based LBL assembly plays a critical role in enhancing the sensitivity of SPR biosensors for the detection of the SORT antigen.[14] Additionally, the decoration of affinity bioreceptors (Anti-SORT antibodies) rather than other types of bioreceptors onto the surface of the LBL nanoassembly can enhance the sensitivity and selectivity of SPR biosensors for detecting SORT antigens in samples owing to their high affinity.[5,7] The utilization of metal nanoparticles directly in the SPR biosensor setup can potentially compromise the stability of the bioconjugate. However, the CH coating serves to bolster the stability of Au-NPs within the solvent system by inducing electrostatic repulsion. Alongside the LBL-based nanoassembly, our

inclination towards employing environmentally friendly plasmonic Au-NPs also contributed to heightened sensitivity. In essence, this eco-friendly synthesis approach for Au-NPs minimizes toxicity to biomolecules, thus preserving their biological functions.

Moreover, the optical characteristics of Au-NPs played a pivotal role in facilitating signal transmission after their interaction with the antigen on the sensor chip.[7] Finally, the inclusion of non-plasmonic 2D modified derivatives of graphene, specifically B-GO nanosheets, in the design of the SPR biosensor for detecting SORT antigen plays a pivotal role due to their unique and versatile properties. In essence, the larger surface area and uniform distribution of carboxylic moieties on B-GO nanosheets facilitate the immobilization of a maximal number of designed nanobioconjugates, thereby enhancing the sensitivity of our SPR biosensor. Additionally, the optical properties and biocompatibility of B-GO nanosheets further contribute to improving the sensitivity of the SPR biosensor.[18] The incorporation of boron as a heteroatom in GO nanosheets enhances both their electrical and optical properties.[30] Hence, the utilization of B-GO nanosheets in the SPR biosensor may offer a viable avenue for enhancing sensitivity to detect low concentrations of the SORT antigen. Overall, the selection of the Au-NPs@CH-PSS-CH-based nanoassembly, environmentally friendly Au-NPs, and B-GO nanosheets based advanced strategies synergistically enhanced the sensitivity and selectivity of the SPR biosensor for SORT antigen detection.

Study of selectivity, spiked samples, and other analytical parameters

Figure 8D demonstrates the remarkable selectivity of the SPR-based biosensor that has been designed. In summary, various interfering agents, such as lysine, glucose, lactoferrin, cholesterol, bovine serum albumin, protease, calcium, sodium, potassium, urea, glycine, and aspartic acid, were introduced. There was no discernible response from the designed SPR biosensor for these interfering agents. Conversely, upon injecting the SORT antigen, a distinct response was observed from the SPR biosensor due to its exceptional selectivity. Furthermore, the response obtained from sample Q closely resembled the response generated by the bare SORT antigen, confirming that other interfering agents within the mixture had no impact on the SPR response. Consequently, this anticipated SPR biosensor validates its potential for application in complex samples.

It is worth noting that the proposed SPR biosensor exhibits a high degree of selectivity exclusively for the SORT antigen. This selectivity is achieved through the use of affinity bioreceptors, specifically Anti-SORT, and the strategic design of LBL-based nanoassemblies. In the case of the CH-based LBL nanoassembly, the uniform amine functionality present on the surface of the LBL nanoassembly provides the necessary orientation, ensuring a high level of selectivity for SORT antigen without any interference from other substances present in the samples. The analysis of SORT antigen-spiked samples was also conducted to validate the practicality of the designed SPR biosensor. Table 1 provides a summary of the percentage recovery of SORT antigen in blood samples. In summary, when 0.4 ng/mL, 0.6 ng/mL, and 0.8 ng/mL of SORT antigen were spiked into plasma samples collected from healthy Wistar albino rats, the recovery rates were 94.06%, 95.2, and 97.48%, respectively. Additionally, the percentage relative standard deviation (% RSD) for spiked samples A, B, and sample C was determined to be 1.55%, 0.83%, and 0.84%, respectively. Notably, the % RSD being less than 5 indicates the excellent practical applicability of the designed SPR-based biosensor for detecting SORT antigen in complex samples such as blood.

Stability and reproducibility analyses of the biosensor play pivotal roles in this research. Table 2 provides a summary of the stability and reproducibility analyses of the SPR biosensor for SORT antigen detection. In short, the stability analysis of the designed SPR biosensor reveals a % RSD of 1.83, which is less than 5 and confirms its excellent stability. The utilization of five SPR biosensors confirmed the recovery of the added amount of SORT antigen (200 pg/mL), resulting in a measured recovery of 196.69 ± 7.55 pg/mL. This finding aligns with the reproducibility analysis, which indicates a recovery rate of 98.34%. The % RSD of 3.84% further confirms the reproducibility of the SPR biosensor for SORT antigen detection, as it falls below the accepted threshold of 5%.
These results collectively validate the reliability and consistency of the designed SPR biosensor in detecting SORT antigen.[31]

Table 1
Percentage recovery of SORT antigen concentrations in spiked blood using SPR biosensor

Sample code	Clinical sample	Concentration of SORT added (ng/mL)	Concentration of SORT found (ng/mL)	% Recovery of SORT	SD	% RSD
A		0.4	0.371	94.06	1.46	1.55
B	Plasma	0.6	0.577	95.2	0.79	0.83
C		0.8	0.784	97.48	0.81	0.84

n = 3; SD (±): Standard deviation; % RSD: % relative SD

Table 2
Stability and reproducibility examination of the SPR biosensor for detection of SORT antigen

Sr. No.	Analytical parameter	Concentration of SORT (pg/mL)		Average % recovery SORT	SD	% RSD
		Added	Found			
1.	Stability	200	196.67 ± 3.61	98.33	1.80	1.83
2.	Reproducibility	200	196.69 ± 7.55	98.34	3.77	3.84

n = 3; SD (±): Standard deviation; % RSD: % relative SD

Possibly, it is due to the design of SPR biosensors incorporating the LBL assembly, B-GO nanosheets, and green-synthesized Au-NPs. The LBL assembly design aids in enhancing selectivity and sensitivity by providing a specific orientation to the antibody, preventing Au-NP aggregation, and offering a smoother surface for antibody immobilization, among other benefits. Overall, the designed SPR biosensor demonstrates good stability and reproducibility.

CONCLUSION

In this research work, we have developed a highly sensitive and selective CH-based LBL nanoassembly decorated on B-GO nanosheets mediated SPR biosensor for the detection of the SORT antigen. To begin, spectral analysis confirmed the formation of 2D hydrophilic, stable, and nanosized non-plasmonic B-GO nanosheets, which were utilized for the immobilization of nanobioconjugates. Here, B-GO nanosheets offer a high surface area, abundant surface functionality for bioconjugate immobilization, excellent biocompatibility, *etc*. The green synthesis method, using an extract from the epicarp of ripe *Terminalia catappa* L. fruit, confirmed the formation of nanosized, eco-friendly, stable, and uniformly dispersed Au-NPs as plasmonic nanomaterials. These green-synthesized Au-NPs not only maintain the biocompatibility of bioreceptors, but also play a crucial role in enhancing the SPR response. Following this, the deposition of CH as a cationic polymer via the LBL nanoassembly approach, based on electrostatic interaction, provides several amine functionalities. These functionalities facilitate the immobilization of Anti-SORT as bioreceptors via carbodiimide chemistry, ensuring specific orientation for Anti-SORT. Consequently, this contributes to the highly selective detection of the SORT antigen. The design of the CH-based polymeric nanoassembly offers a softer surface for the immobilization of Anti-SORT, helping to preserve the biofunctionality of biomolecules and further enhancing sensitivity. As a result, the designed SPR biosensor offers a wide linear range (400 ng/mL to 0.1 ng/mL), a low detection limit for SORT antigen (6.09 pg/mL), high selectivity, good stability, practicality, and reproducibility. The preference for CH-based nanoassembly, environmentally friendly Au-NPs, and B-GO nanosheets collectively enhances the overall performance of the SPR biosensor. In conclusion, this CH-mediated nanobioconjugate and B-GO nanosheets-based SPR biosensor design offers high sensitivity, selectivity, simplicity, cost-effectiveness, eco-friendliness, minimally invasive detection, label-free operation, stability, and reproducibility. It serves as a viable alternative for the detection of the SORT antigen, contributing to the *in vitro* diagnosis of CAD.

ACKNOWLEDGMENT: The authors wish to extend their gratitude to the Indian Council of Medical Research (ICMR), New Delhi, for providing the Research Associate (RA) fellowship (File No.: 3/1/1(27)/2022-NCD-I). Special thanks are due to the Sophisticated Test and

Instrumentation Centre (STIC), Cochin University of Science and Technology, Cochin: 682 022, Kerala, India, for providing essential spectroscopic characterization facilities. Additionally, the authors are thankful to the Indian Institute of Technology (IIT), Roorkee, India, for their assistance with XPS characterization. Furthermore, the authors express their appreciation to the Principal, Dr. S. B. Bari, and the Management of the H. R. Patel Institute of Pharmaceutical Education and Research in Shirpur for generously providing the necessary infrastructure and resources for this research.

REFERENCES

[1] J. Xue, Y. Zhang, Z. Guang, T. Miao, Z. Ali *et al*., *Sensors*, **23**, 2020 (2023), https://doi.org/10.3390/s23042020
[2] M. Ullah, A. Wahab, S. U. Khan, U. Zaman, K. Rehman *et al*., *Curr. Probl. Cardiol*., **48**, 101415 (2023), https://doi.org/10.1016/j.cpcardiol.2022.101415
[3] R. H. Werida, A. Omran and N. M. El-Khodary, *Int. J. Gen. Med*., **14**, 6167 (2021), https://doi.org/10.2147/IJGM.S324889
[4] L. Tang, J. Yang, Y. Wang and R. Deng, *ACS Sens*., **8**, 956 (2023), https://doi.org/10.1021/acssensors.2c02311
[5] S. Nangare and P. Patil, *Crit. Rev. Anal. Chem*., **52**, 1139 (2022), https://doi.org/10.1080/10408347.2020.1864716
[6] P. L. Møller, P. D. Rohde, S. Winther, P. Breining, L. Nissen *et al*., *Front. Cardiovasc. Med*., **8**, 652584 (2021), https://doi.org/10.3389/fcvm.2021.652584
[7] S. N. Nangare and P. O. Patil, *ACS Biomater. Sci. Eng*., **7**, 2 (2020), https://doi.org/10.1021/acsbiomaterials.0c01203
[8] S. Nangare and P. Patil, *Crit. Rev. Anal. Chem*., **53**, 1 (2023), https://doi.org/10.1080/10408347.2021.1927669
[9] P. O. Patil, G. R. Pandey, A. G. Patil, V. B. Borse, P. K. Deshmukh *et al*., *Biosens. Bioelectron*., **139**, 111324 (2019), https://doi.org/10.1016/j.bios.2019.111324
[10] S. Nangare and P. Patil, *Anal. Chim. Acta*, **1271**, 341474 (2023), https://doi.org/10.1016/j.aca.2023.341474
[11] M. M. Barsan and C. M. Brett, *TrAC Trends Anal. Chem*., **79**, 286 (2016), https://doi.org/10.1016/j.trac.2015.11.019
[12] S. Nangare and P. Patil, *Int. J. Biol. Macromol*., **250**, 126224 (2023), https://doi.org/10.1016/j.ijbiomac.2023.126224
[13] Z. Zhao, Q. Li, J. Gong, Z. Li and J. Zhang, *RSC Adv*., **10**, 17731 (2020), https://doi.org/10.1039/D0RA02474K
[14] B. Masereel, M. Dinguizli, C. Bouzin, N. Moniotte, O. Feron *et al*., *J. Nanopart. Res*., **13**, 1573 (2011), https://doi.org/10.1007/s11051-010-9908-3
[15] S. Amirthalingam and J. Rangasamy, in "Chitosan for Biomaterials III: Structure–Property Relationships", edited by R. Jayakumar and M. Prabaharan, Springer, 2021, p. 233, https://doi.org/10.1007/12_2021_85
[16] M. Junaid, M. M. Khir, G. Witjaksono, N. Tansu, M. S. M. Saheed *et al*., *Molecules*, **25**, 3646 (2020), https://doi.org/10.3390/molecules25163646
[17] D. D. Borhade, S. N. Nangare, D. A. Patil, P. O. Patil, G. S. Patil *et al*., *J. Drug Deliv. Sci. Technol*., **82**, 104325 (2023), https://doi.org/10.1016/j.jddst.2023.104325
[18] V. Thirumal, A. Pandurangan, R. Jayavel and R. Ilangovan, *Synth. Met*., **220**, 524 (2016), https://doi.org/10.1016/j.synthmet.2016.07.011
[19] T. Powar, A. Hajare, R. Jarag and S. Nangare, *Acta Chim. Slov*., **68**, 861 (2021), https://doi.org/10.17344/acsi.2021.6858
[20] D. Philip, *Phys. E: Low-Dimens. Syst. Nanostruct*., **42**, 1417 (2010), https://doi.org/10.1016/j.physe.2009.11.081
[21] M. Sahoo, K. Sreena, B. Vinayan and S. Ramaprabhu, *Mater. Res. Bull*., **61**, 383 (2015), https://doi.org/10.1016/j.materresbull.2014.10.049
[22] M. Singh, R. Kalaivani, S. Manikandan, N. Sangeetha and A. Kumaraguru, *Appl. Nanosci*., **3**, 145 (2013), https://doi.org/10.1007/s13204-012-0115-7
[23] S. Smitha, D. Philip and K. Gopchandran, *Spectrochim. Acta A: Mol. Biomol. Spectrosc*., **74**, 735 (2009), https://doi.org/10.1016/j.saa.2009.08.007
[24] G. Das, S. Seo, I.-J. Yang, L. T. H. Nguyen, H.-S. Shin *et al*., *Int. J. Nanomed*., **18**, 17 (2023), https://doi.org/10.2147/IJN.S378806
[25] O. M. El-Borady, M. Fawzy and M. Hosny, *Appl. Nanosci*., **13**, 3149 (2023), https://doi.org/10.1007/s13204-021-01776-w
[26] S. Satpathy, A. Patra, B. Ahirwar and M. D. Hussain, *Phys. E: Low-Dimens. Syst. Nanostruct*., **121**, 113830 (2020), https://doi.org/10.1016/j.physe.2019.113830
[27] K. X. Lee, K. Shameli, M. Miyake, N. Kuwano, N. B. Bt Ahmad Khairudin *et al*., *J. Nanomater*., **2016**, 8489094 (2016), https://doi.org/10.1155/2016/8489094
[28] G. Devendrapandi, M. I. Sahay, D. Padmanaban, A. Panneerselvam, R. Palraj *et al*., *Inorg. Chem. Commun*., **151**, 110636 (2023), https://doi.org/10.1016/j.inoche.2023.110636
[29] A.-N. D. Egueh, B. Lakard, P. Fievet, S. Lakard and C. Buron, *J. Colloid Interface Sci*., **344**, 221 (2010), https://doi.org/10.1016/j.jcis.2009.12.033
[30] T. Van Khai, H. G. Na, D. S. Kwak, Y. J. Kwon, H. Ham *et al*., *J. Chem. Eng*., **211**, 369 (2012), https://doi.org/10.1016/j.cej.2012.09.081
[31] S. Nangare, K. Chaudhari and P. Patil, *J. Photochem. Photobiol. A: Chem*., **446**, 115158 (2024), https://doi.org/10.1016/j.jphotochem.2023.115158